

Load Sequence Effects in the Fatigue Design of Welded Spatial Tubular Joints in Jackets

Prof. Dr.-Ing. Peter Schaumann, Dipl.-Ing. Alexander Raba, Dipl.-Ing. Stephan Lochte-Holtgreven
ForWind Center for Wind Energy Research, Institute for Steel Construction
Leibniz Universitaet Hannover, Germany

ABSTRACT

The fatigue performance of components in substructures of offshore wind turbine generators is decisive for the design. Current standardised fatigue assessment approaches neglect load history dependant material behaviour and estimate a linear dependence between stresses and strains. The present paper lines out basic theoretical considerations about effects of varying load sequences and shows investigations considering their relevance to welded spatial tubular joints in jacket substructures. All conducted investigations are based on the Uniform Material Law and on relevant technical guidelines for substructures of offshore wind turbine generators.

KEY WORDS: Fatigue; sequence effects; load history; cyclic loading; tubular joints; offshore wind energy.

INTRODUCTION

Support structures of offshore wind turbines (OWT) are exposed to a combination of arbitrary wind and wave loads. During a desired lifetime of 25 to 30 years these structures have to endure enormous amounts of cyclic excitations which cause material fatigue. In the majority of cases the bearing capacity of a support structure is limited by its fatigue performance.

Other than material's ultimate strength, the material and structural fatigue strength depends decisively on:

- notch effects,
- surface roughness,
- mean stress,
- temperature, and
- corrosion.

As a result, fatigue strength shows a much greater deviation throughout the same base material than the material's ultimate strength.

Especially welded spatial tubular joints, as they can be found in jacket substructures (Fig. 1) are exposed to fatigue. The spatial intersection leads to complex interference of stresses. Moreover, in the weakest point of the intersection stresses have to be transferred between the

tubes by welds. Welding inevitably cause embrittlement of the material, residual stresses and notches at the surface. These effects have to be covered by a fatigue assessment.

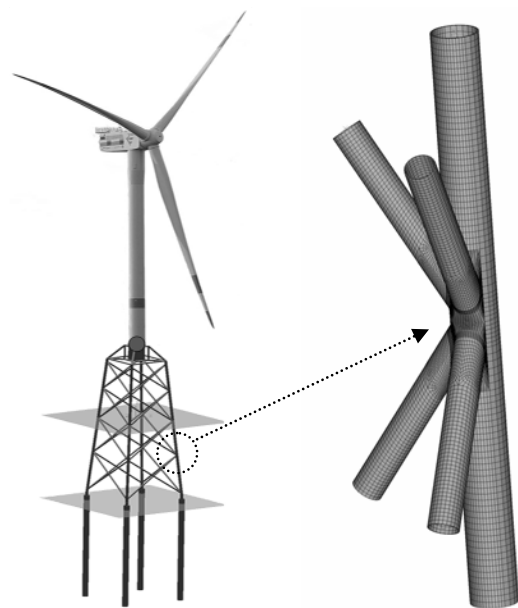


Fig. 1. Offshore wind turbine with jacket substructure (Schaumann, 2010) and detail of a double K-Joint.

Today several methods for a fatigue assessment are available, e.g. structural-stress approach or notch-strain approach. However, only few methods are part of standards and certification guidelines. In the field of offshore substructures, the structural-stress approach is state of the art.

In order to reduce the expenses of assessing fatigue performance some basic simplifications are part of current approaches. Regarding load patterns it is the application of counting methods and therefore neglecting the chronology of events. Regarding material behaviour it is the assumption of a linear stress-strain relation. As a result, to identify the

influence of load patterns with similar loads but different chronologies, counting methods must be skipped and a load history dependent material law has to be utilised.

UNIFORM MATERIAL LAW

For the conducted investigations the authors chose the Uniform Material Law (UML) published by Bäuml and Seeger (1990). The UML is a combination of equations, rules, and tabulated parameters. Supplementary provisions are stated in Radaj, Sonsino and Fricke (2006) or Gudehus and Zenner (1999) and were also considered. Hence, the UML used within the following examinations consists of:

- constitutive equations for the stress-strain relation,
- memory effects describing load history dependent behaviour,
- a constitutive equation for a strain Wöhler curve and
- tabulated material parameters.

Design basis for the UML are on uniaxial cyclic loading tests of specimen with a high length to diameter ratio, similar to the model concept of the notch-strain approach. Therefore the following constitutive equations are one-dimensional.

Cyclic stress-strain curve

The basic stress-strain relation, the cyclic stress-strain curve (CSSC) is based on a formulation by Ramberg and Osgood (1943) and is given in Eq. (1) (cf. Fig. 2, solid line).

$$\varepsilon = \varepsilon_{el} + \varepsilon_{pl} = \frac{\sigma}{E} + \left(\frac{\sigma}{K^I} \right)^{\frac{1}{n^I}} \quad (1)$$

The total strain is a combination of elastic ε_{el} and plastic ε_{pl} strains. Whereas the elastic strain ε_{el} is calculated according to Hooke's law as quotient of stress σ and Young's modulus E . And the plastic strain ε_{pl} is the quotient of stress σ and cyclic strain-hardening coefficient K^I , to the power of the reciprocal value of the cyclic strain-hardening exponent n^I .

This is the initial path for the stress-strain relation when starting to load.

Hysteresis branch

After reaching a maximum load (load reversal point, l_{rp}) on the CSSC, an unloading process is going to be introduced. During the unloading process, plastic deformations remain in the material and only elastic deformations vanish until a total unloading. Subsequent loading in the opposite direction introduces plastic strains again. This load history dependent behaviour is known as hysteresis. The hysteresis branch (HB) can be described by Eq. (2) (cf. Fig. 2, dotted line).

$$\varepsilon = \varepsilon_{l_{rp}} + \frac{\sigma - \sigma_{l_{rp}}}{E} + 2 \left(\frac{\sigma - \sigma_{l_{rp}}}{2K^I} \right)^{\frac{1}{n^I}} \quad (2)$$

Eq. (2) is based on a formulation by Masing (1926) and corresponds to Eq. (1), shifted to the load reversal point $(\varepsilon_{l_{rp}}, \sigma_{l_{rp}})$. The doubling of plastic strain covers kinematic hardening.

Memory effects

Certain rules describing the load history dependent material behaviour are stated by e.g. Gudehus and Zenner (1999) or Haibach (2006) and have to be observed.

- Memory 1 (M1): After closing a hysteresis loop that started on the cyclic stress-strain curve, the stress-strain path returns to the cyclic stress-strain curve (cf. Fig. 2, path 1-2-1).
- Memory 2 (M2): After closing a hysteresis loop that started on a hysteresis branch, the stress-strain path returns to the previous hysteresis branch (cf. Fig. 2, path 4-5-4).
- Memory 3 (M3): If a hysteresis branch that started on the cyclic stress-strain curve exceeds the absolute value of its starting point on the opposite side, the stress-strain path returns to the cyclic stress-strain curve (cf. Fig. 2, path 3-6 and 7-8). This hysteresis branch will stay unclosed.

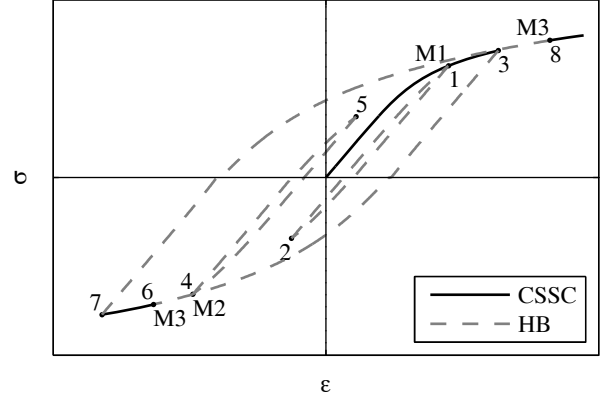


Fig. 2. Stress-strain plot of UML.

Strain Wöhler curve

The stress-strain relation can be fully described by implementing the previously introduced equations and rules in a numerical design tool. However, Wöhler curves are needed for a fatigue assessment. Based on a formulation by Manson and Coffin (cf. Gudehus & Zenner, 1999) strain Wöhler curves for the UML can be calculated according to Eq. (3). Mean stress effects described by Morrow (1965) are included in Eq. (3).

$$\varepsilon_a = \varepsilon_{a,el} + \varepsilon_{a,pl} = \frac{\sigma_f' - \sigma_m}{E} (2N)^b + \varepsilon_f' (2N)^c \quad (3)$$

These strain Wöhler curves are the sum of elastic ε_{el} and plastic strains ε_{pl} and depend on the number of cycles N . The mean stress σ_m is included in the elastic strain as well. Besides the Young's modulus E the material properties are described by the fatigue strength coefficient σ_f' and exponent b , as well as the fatigue ductility coefficient ε_f' and exponent c .

A parameter comparison of Eq. (1) equated with Eq. (3) leads to the following assumptions (cf. Gudehus and Zenner, 1999):

$$n^I = \frac{b}{c} \quad (4)$$

$$K^I = \frac{\sigma_f'}{(\varepsilon_f')^{n^I}} \quad (5)$$

Cyclic material parameters

In order to solve the introduced equations a set of parameters was published by Bäuml and Seeger (1990). These parameters result from

several material tests of uniaxially loaded specimen and a best fit analysis and therefore, can be assumed to be well validated. Parameters for unalloyed and low alloyed steel are given in Table 1.

Table 1. Cyclic material parameters of unalloyed and low alloyed steel (Bäumel and Seeger, 1990).

$\sigma_f^l = 1.50 \cdot \sigma_u$	Fatigue strength coefficient
$b = -0.087$	Fatigue strength exponent
$\varepsilon_f^l = 0.59 \cdot \psi$	Fatigue ductility coefficient
$c = -0.58$	Fatigue ductility exponent
$\sigma_E = 0.45 \cdot \sigma_u$	Technical stress endurance limit
$\varepsilon_E = 0.45 \cdot \frac{\sigma_u}{E} + 1.95 \cdot 10^{-4} \cdot \psi$	Technical strain endurance limit
$N_E = 5 \cdot 10^5$	Number of full cycles at technical endurance limit
$K^l = 1.65 \cdot \sigma_u$	Cyclic strain-hardening coefficient
$n^l = 0.15$	Cyclic strain-hardening exponent
$\psi = \begin{cases} 1.0 & \text{for } \frac{\sigma_u}{E} \leq 3 \cdot 10^{-3} \\ \left(1.375 - 125 \cdot \frac{\sigma_u}{E}\right) \leq 0 & \text{for } \frac{\sigma_u}{E} > 3 \cdot 10^{-3} \end{cases}$	

Implementation

A one-dimensional formulation of the UML was implemented in ANSYS® User Programmable Feature (UPF) for a LINK180 spar element. Besides the stress-strain relation, the overall damage for each load step can be calculated at run-time. Based on the implemented material law, load sequence effects in general can be investigated.

LOAD SEQUENCE EFFECTS

Load sequence effects were examined using UML calculations compared to calculations of a bi-linear material law including kinematic hardening (BKIN). The material properties correspond to a S355 structural steel with a plate thickness $t < 100$ mm (EN 10225, 2009).

Maximum load

Both material laws contain elastic strains correspondent to Hooke's law; the UML moreover includes plastic strains (Eq. (1)). To obtain the yield stress level f_y from test data the yield stress level is defined at a plastic strain of:

$$\frac{\varepsilon_{pl}(f_y)}{\varepsilon(f_y)} = \frac{\left(\frac{f_y}{K^l}\right)^{1/n^l}}{\left(\frac{f_y}{E}\right) + \left(\frac{f_y}{K^l}\right)^{1/n^l}} = 0.2\% . \quad (6)$$

Therefore, different results between UML and BKIN are apparent for stress levels beyond the following limit:

$$f_{y,UML} = 101.26 \text{ MPa} . \quad (7)$$

While the BKIN is based on loading tests with increased load until rupture, the UML is a best fit regression of the stress-strain relation after several thousand load cycles. And since the yield plateau, distinc-

tive within a static loading test, disappears after initial load cycles, the yield stress of the UML is fairly low compared to the BKIN. In order to cause plastifications, the maximum loads for the following examinations are chosen accordingly.

Load patterns

To examine effects of different load sequences, a set of artificial load patterns was generated. These patterns differ in their sequences but lead to equal rainflow matrices when applying the Rainflow HCM (Clorrmann and Seeger, 1986). Choosing load patterns with different sequences but equal rainflow matrices allows examining sequence effects only. This is due to the fact that similar rainflow matrices will lead to same damage values. The generated load patterns are varied by the following aspects:

- position of a single primary peak,
- position of two single primary peaks with equal signs,
- position of two single primary peaks with different signs,
- amplitude of secondary peaks (in- or outside plastic range), and
- mean load level.

All investigations were conducted strain and stress-driven, as well as with inversed amplitudes. For the sake of clarity the values are plotted continuously instead of discrete and almost only strain-driven results are presented.

Single primary peak

When the primary peak exceeds the elastic limit, plastic deformations occur causing a lower stress maximum than calculated by the BKIN material law (Fig. 3). The stress difference between UML and BKIN stays impressed in the material by means of a mean stress. Thereby the sign of the mean stress level is opposite to the peak which caused plastification. The subsequent secondary peaks lead to purely elastic material behaviour, as could be expected. Inversed amplitudes lead to an inversed mean stress level (Fig. 4).

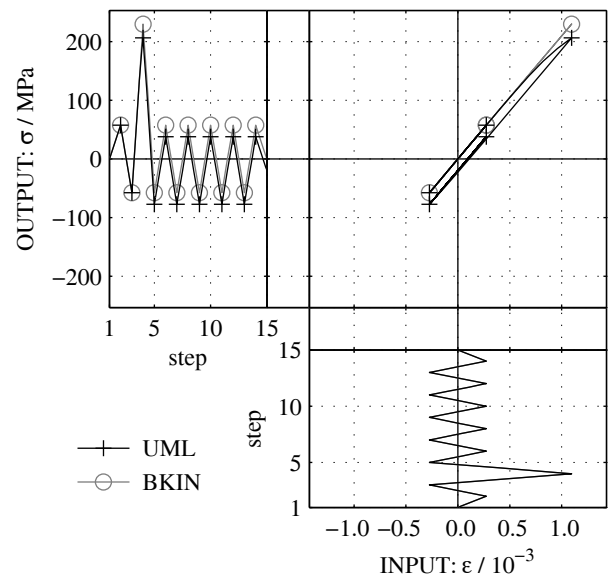


Fig. 3. Stress-strain relation for a stress-driven calculation of a load pattern with an early positive primary peak.

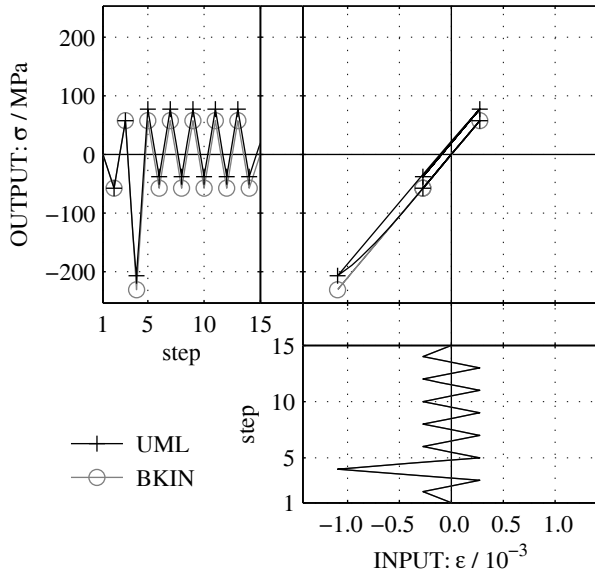


Fig. 4. Stress-strain relation for a stress-driven calculation of a load pattern with an early negative primary peak.

Stress- or strain-driven

While in a strain-driven calculation plastification leads to a mean stress level inverse to the plastic peak, a stress-driven calculation leads to a mean strain level in the same direction as the plastic peak (Fig. 5).

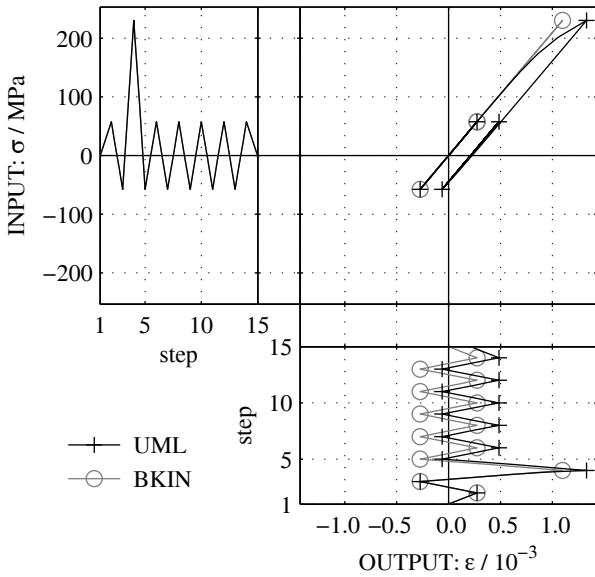


Fig. 5. Stress-strain relation for a strain-driven calculation of a load pattern with an early primary peak.

Position of a single primary peak

Despite the strain or stress-driven calculation, the effect of a plastic primary peak in a total elastic set of secondary peaks is independent of the chronology of peaks (Fig. 3~5). Nevertheless, the period with a mean strain or stress level differs.

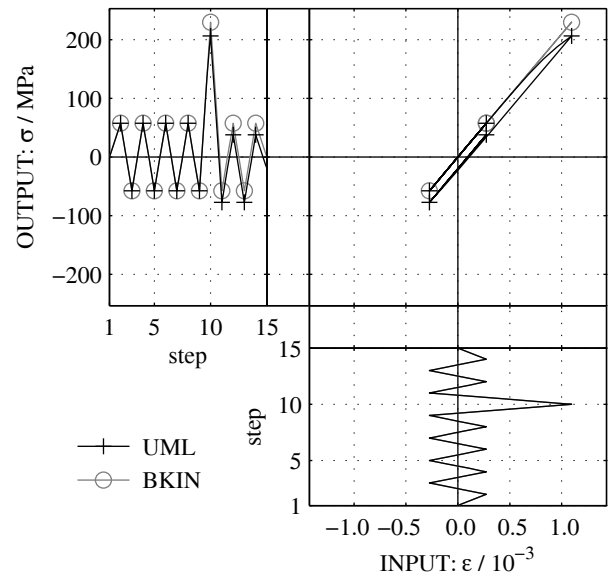


Fig. 6. Stress-strain relation for a stress-driven calculation of a load pattern with a late primary peak.

Position of two single primary peaks with equal signs

No further plastic strains are caused until the initial plastic zone is exceeded again after initial plastification (Fig. 7). This is predictable as the hysteresis loop shows a kind of a delay in the stress-strain relation but no plastic increase in the direction of the initial plastification.

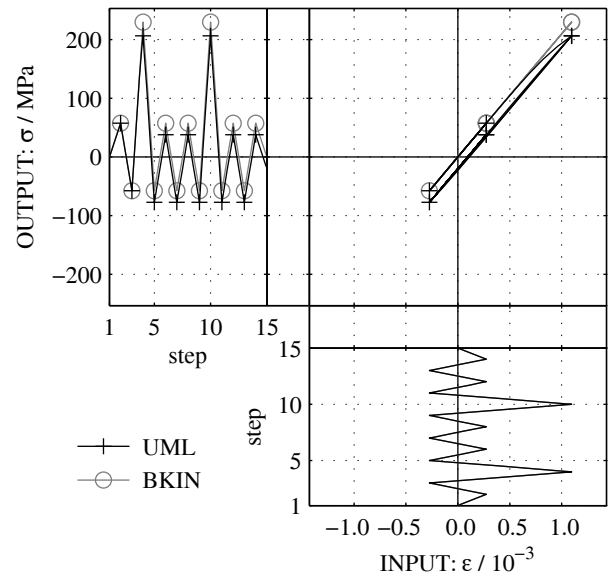


Fig. 7. Stress-strain relation for a strain-driven calculation of a load pattern with two single primary peaks with equal signs.

Position of two single primary peaks with different signs

A second primary peak with a different sign than the first primary peak leads to plastic deformations on the opposite side (Fig. 8). Each primary peak on its own induces the same effect as described before. But exceeding the elastic limit in the opposite direction of a prior primary peak reverses the sign of the mean strain level. Therefore, plastic load-

ing in one direction cannot be reset to zero by loading with the same amplitude to the opposite direction. This behaviour corresponds to kinematic hardening.

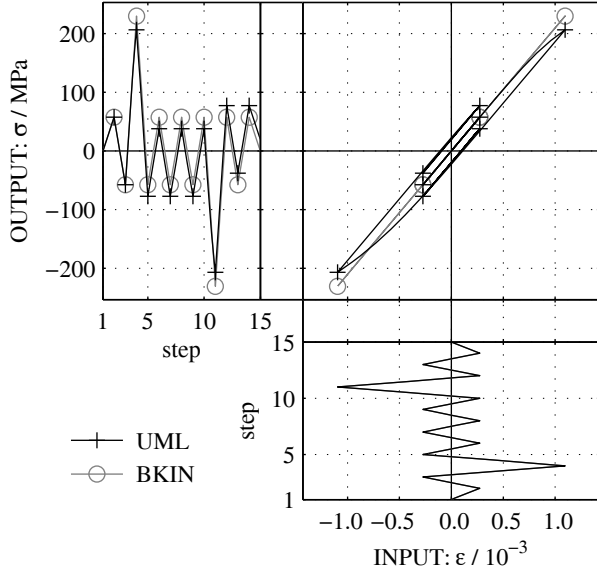


Fig. 8. Stress-strain relation for a strain-driven calculation of a load pattern with two single primary peaks with opposite signs.

Amplitude of secondary peaks

Additionally to a primary peak, increasing the amplitude of secondary peaks above the purely elastic range leads to a constant reduction of the mean stress level. This reduction is caused by plastification in the opposite direction of the primary peak (Fig. 9). Other than that, no further effects are visible.

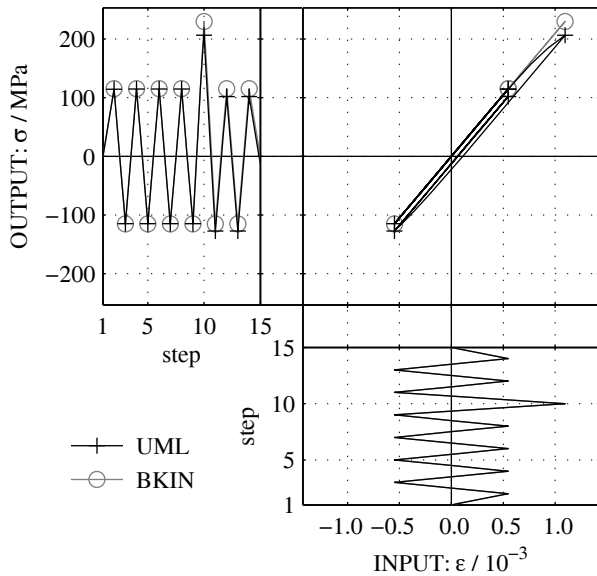


Fig. 9. Stress-strain relation for a strain-driven calculation of a load pattern with a single primary peak and plastic secondary peaks.

Mean load level

A constant mean load level shows no significantly new findings. But in Fig. 10 an increase in the mean stress level is already perceptible after the first load peak. This corresponds to prior statements.

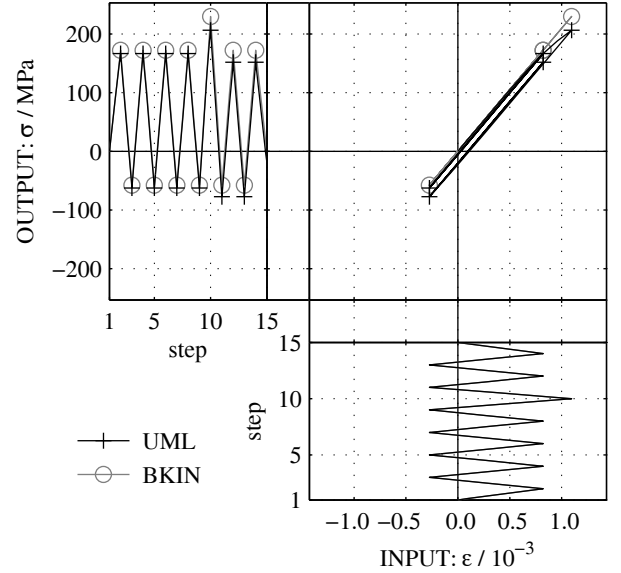


Fig. 10. Stress-strain relation for a strain-driven calculation of a load pattern with a single primary peak, plastic secondary peaks and a constant mean strain.

Damage

Damage estimations for the presented load patterns were calculated in three ways. In the first place, the Manson and Coffin (MC) equation (Eq. (3)) was solved for the maximum number of endurable cycles N per hysteresis loop and the result was inserted in Miner's sum (Eq. (8)).

$$D = \sum_i \frac{n_i}{N_i} \quad (8)$$

The damage D is the sum of the quotient of number of effective cycles n_i and maximum amount of endurable cycles N_i per similar hysteresis loop.

In the second place, the damage parameter P_{SWT} by Smith, Watson and Topper (SWT) (1970) was calculated (Eq. (9)).

$$P_{SWT} = \sqrt{(\sigma_a + \sigma_m) \cdot \varepsilon_a \cdot E} \quad (9)$$

The damage parameter P_{SWT} depends on the stress amplitude σ_a and mean value σ_m , as well as the strain amplitude ε_a . The resulting damage was estimated by equating Eq. (10) with the previously calculated parameter P_{SWT} and solving it for the maximum number of endurable cycles N per hysteresis loop.

$$P_{SWT} = \sqrt{(\sigma_f^t)^2 \cdot (2N)^{2b} + \sigma_f^t \cdot \varepsilon_f^t \cdot E \cdot (2N)^{b+c}} \quad (10)$$

Eq. (10) includes the same parameters as the Manson and Coffin Eq. (3). The estimated damages are shown in Fig. 12 and Table 5. Both ways of calculation show significant effects on the damage sum when taking load sequence effects into account. A compressive mean stress

introduced by plastification reduces damage significantly. Whereas a tensile mean stress leads to an increase of damage. This corresponds to the general comprehension of tensile stresses to be mainly relevant for fatigue.

The damage parameter by Smith, Watson and Topper is more sensitive towards tensile mean stresses than Manson and Coffin (cf. Table 5: Fig. 4 and Fig. 8).

In the third place, the damage was calculated according to DNV-OS-J101 (2010) standard, which will be described in the following.

RELEVANCE FOR SPATIAL TUBULAR JOINTS

To estimate the relevance of previous observations for spatial tubular joints, as they can be found in jackets, it was examined to what extent different results can be expected for an UML based calculation in comparison to current standard conform approaches.

The frequency of fatigue relevant loads in an OWT substructure can be assumed to be in range of the first eigenfrequency. For most OWTs founded on jackets this frequency is about $f=0.26\text{ Hz}$ (cf. Böker, 2009). Hence, the maximum number of endurable load cycles in a lifetime of 25 years will be assumed to:

$$N = 0.26 \cdot 60 \cdot 60 \cdot 24 \cdot 365 \cdot 25 \approx 2 \cdot 10^8. \quad (11)$$

As already mentioned, current state-of-the-art method for fatigue assessment of jacket structures is the structural stress approach (cf. DNV-OS-J101, 2010). Utilising both counting methods and a linear material law, different results for a standard conform and an UML calculation have to be expected.

For fatigue assessment of tubular joints the DNV-OS-J101 (2010) defines three different S-N-curves, which depend on environmental conditions. They can be calculated by Eq. (12) using the parameters tabulated in Table 2. The resulting curves are plotted in Fig. 11.

Table 2. S-N curve parameters to solve Eq. (12). (DNV-OS-J101, 2010)

Structural detail	Environment											
	In air				In seawater with corrosion protection				Free corrosion			
	$\log_{10}(a)$	m	Range of validity	k	$\log_{10}(a)$	m	Range of validity	k	$\log_{10}(a)$	m	k	
Weld in tubular joint (acc. to Fig. 1)	12.164	3	$N < 10^7$	0.25	11.764	3	$N < 10^6$	0.25	11.687	3	0.25	
	15.606	5	$N > 10^7$	0.25	15.606	5	$N < 10^6$	0.25				

Table 3. Definition of design fatigue factors. (DNV-OS-J101, 2010)

Location	Accessibility for inspection and repair of initial fatigue and coating damages	Corrosion protection	Corrosion allowance	S-N curve	DFF
Atmospheric zone	Yes	Coating	No	In air	1.0
Splash zone	Yes	Coating	Yes	Combination of curves marked "air" and "free corrosion"	2.0
	No				3.0
Submerged zone	Yes	Cathodic protection and optional coating	No	In seawater	2.0
	No				3.0
Scour zone	No	None	Yes		3.0
Below seabed	No		No		3.0
Closed compartments with seawater	Yes	Cathodic protection, coating near free surfaces and above free surfaces	Yes		2.0
	No				3.0

$$\log_{10}(N) = \log_{10}(a) - m \cdot \log_{10} \left(\Delta \sigma \cdot \left(\frac{t}{t_{ref}} \right)^k \right) \quad (12)$$

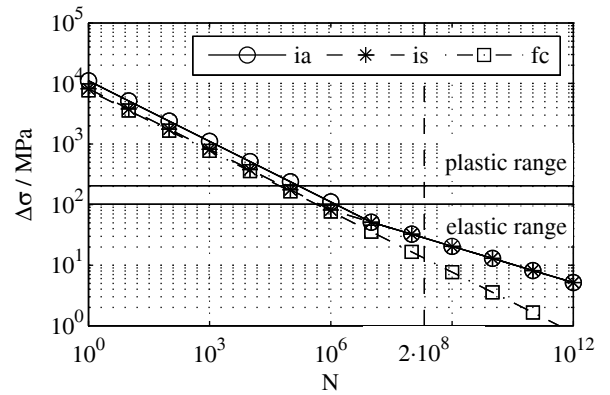


Fig. 11. Characteristic S-N-curves for a thickness of 35 mm according to DNV-OS-J101 (2010). (ia: in air; is: in seawater; fc: free corrosion)

The overall damage is calculated by Miner's sum (cf. Eq. (8)) including design fatigue factors (DFF). Two different methods to include the DFF are available in DNV-OS-J101 (2010). Method 2, which considers the DFF by partial safety factors for the material, will be used in the following. The factors dependent on environmental conditions are presented in Table 3 and Table 4.

Table 4. Material partial safety factors. (DNV-OS-J101, 2010)

DFF	γ_m
1.0	1.0
2.0	1.15
3.0	1.25

Considering that a single peak above the yield stress $f_{y,UML}$ introduces a constant mean stress level (cf. Fig. 3), the characteristic S-N curves plotted in fig. 11 do not exclude plastic deformations. Dependent on maximum amplitude and mean value these S-N curves allow almost $N = 10^5$ cycles within the UML's total plastic range and up to $N = 10^6$ cycles within the UML's elastic-plastic range. Considering the most conservative DFF of 3.0, about $N = 8 \cdot 10^4$ cycles within the UML's elastic-plastic range are still admissible.

For a cyclic load with constant amplitude and a frequency of $f = 0.26 \text{ Hz}$ a stress-range of about $\Delta\sigma = 10 \text{ N/mm}^2$ is admissible in free corrosion conditions for a life-time of 25 years. Therefore, a numerical example was conducted. An artificial load pattern (LC1) with secondary peaks at $\sigma = \pm 5 \text{ N/mm}^2$ and a primary peak at $\sigma = 150 \text{ N/mm}^2$ in every 4000th cycle, similar to the load pattern plotted in Fig. 7, leads to a damage of $D = 0.85$ according to DNV-OS-J101 (2010) (cf. Table 5). The same load pattern but with inversed amplitudes (LC2) leads to the same result according to DNV-OS-J101 (2010).

Damage estimations according to MC or SWT were between 10^{-4} and 10^{-8} times lower (cf. Table 5) for all presented load patterns. Especially for the last two load patterns the difference in the MC and SWT damage sum caused by the negative mean stress level was remarkable.

CONCLUSION AND OUTLOOK

The investigations carried out elucidate effects of different load sequences. As expected, an effect is evident and becomes apparent by

means of a mean level. Decisive for the mean load level are the previous extreme values, as well as the way of calculating (i.e. stress or strain-driven). After an initial plastification in one direction, the generated mean level can only be changed by a further plastification in the same direction or by an initial plastification in the opposite direction.

In case of a strain-driven calculation the mean stress level is on the opposite side of the crucial load reversal point. Hence the commonly used BKIN, compared to the UML, overestimates the maximum stress level in a cyclic loading test (cf. Fig. 3). In case of a stress-driven calculation the mean strain level is on the same side as the crucial load reversal point and the BKIN underestimates the maximum strain levels (cf. Fig. 5).

These effects have an impact on the fatigue performance. Fatigue sensitive areas mainly bear notches or micro cracks. These cracks grow under tensile loading. Because the crack surfaces cannot convey tensile loads, the dedicated loads focus in the crack root and overload the material.

A compressive mean load level, regardless of stress or strain, improves the fatigue performance because cracks do not open as far as without a compressive mean load level. In contrast to that, a tensile mean load level decreases the fatigue strength because cracks will remain open. Thus this negative effect has to be included in damage estimation.

Even though these results are based on well validated material laws, they are numerical results and therefore only show differences between

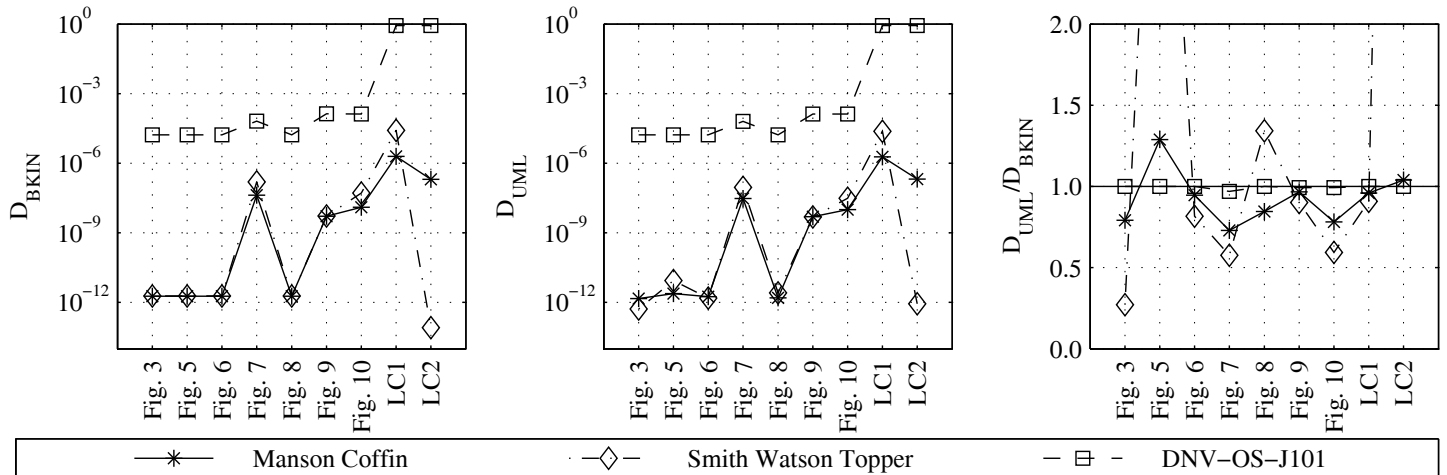


Fig. 12. Plots of damage estimations for presented results, given in Table 5.

Table 5. Damage estimations for results presented in Fig. 12.

	Fig. 3	Fig. 4	Fig. 6	Fig. 7	Fig. 8	Fig. 9	Fig. 10	LC1	LC2	
MC	D_{BKIN}	1.87E-12	1.87E-12	1.87E-12	4.18E-08	1.87E-12	5.18E-09	1.27E-08	1.95E-06	2.01E-07
	D_{UML}	1.48E-12	2.41E-12	1.77E-12	3.05E-08	1.58E-12	5.01E-09	9.93E-09	1.87E-06	2.09E-07
	D_{UML}/D_{BKIN}	0.79	1.29	0.95	0.73	0.84	0.97	0.78	0.96	1.04
SWT	D_{BKIN}	1.90E-12	1.90E-12	1.90E-12	1.57E-07	1.90E-12	5.33E-09	5.19E-08	2.61E-05	8.19E-14
	D_{UML}	5.17E-13	8.65E-12	1.55E-12	9.05E-08	2.55E-12	4.80E-09	3.08E-08	2.37E-05	8.70E-13
	D_{UML}/D_{BKIN}	0.27	4.55	0.82	0.58	1.34	0.90	0.59	0.91	10.62
DNV	D_{BKIN}	1.67E-05	1.67E-05	1.67E-05	6.54E-05	1.67E-05	1.34E-04	1.33E-04	8.55E-01	8.55E-01
	D_{UML}	1.67E-05	1.67E-05	1.67E-05	6.34E-05	1.67E-05	1.33E-04	1.32E-04	8.55E-01	8.55E-01
	D_{UML}/D_{BKIN}	1.00	1.00	1.00	0.97	1.00	1.00	0.99	1.00	1.00

theoretical formulations. Moreover additional cyclic effects, i.e. mean stress relaxation and mean strain creep (cf. e.g. Radaj, Sonsino and Fricke, 2006 or Gudehus and Zenner, 1999), are not included in the implementation but might have a significant effect on the results.

The numerical example presented in the end concludes that load sequence effects are not excluded in a current standard conform fatigue assessment. Certainly stress ranges with constant amplitude within the UML's plastic range are not admissible for a lifetime of 25 years, but the investigations of simple load patterns show significant effects for single peaks above the elastic range.

Comparing the damage sums of the DNV to the damage sums of MC or SWT leads to the conclusion that DNV is on the safe side since it is rather conservative. This might also be the reason for the approved reliability of the structural stress approach. Moreover mean stress relaxation and mean strain creep might reduce both positive and negative effects of plastification by reducing the mean threshold over time.

All presented investigations are conducted for artificial load patterns and with the assumption of a stress and strain free specimen. For application on real structures two unavoidable circumstances need to be considered. On the one hand manufacturing processes such as forming and welding will introduce stresses to the material that need to be included in a UML calculation. And on the other hand wind and wave loads are totally arbitrary and therefore are not predictable in detail. So for example, when designing a structure for a load pattern that introduces a compressive mean stress in the beginning of the life-time, the fatigue performance will be overestimated if the plastification stays out.

SUMMARY

In this paper, the effects of load sequences on the fatigue performance of welded spatial tubular joints were investigated. The current state-of-the-art approach for a fatigue assessment does not consider load sequence effects. A one-dimensional version of the Uniform Material Law according to Bäumel and Seeger was implemented in the ANSYS® User Programmable Feature. Based on this implementation, simple artificial load patterns with different load chronologies were investigated by their resulting stress-strain relations. Finally, the relevance of load sequence effects to the current standard fatigue assessment was estimated.

The UML shows a low yield strength and therefore plastification at lower stress levels than the bilinear material law. As a result, single peaks above the yield level lead to a shift in the mean values. In stress-driven calculations a strain mean level and in strain-driven calculations a stress mean level occurs having a positive or negative influence on the fatigue performance depending on whether they are tensile or compressive.

A practical consideration of load sequence effects is possible, but needs particular attention. In general, it is important to precisely describe the load chronology and the maximum peaks. This is only possible for a design process if stochastic deviations of the load can be excluded. Otherwise severe over- or underestimations of the fatigue life will be the result. For a re-evaluation of an existing structure, where a precise load history is available, load sequence effects can be considered and a fatigue life prolongation can be investigated. Nevertheless, including load sequence effects in a fatigue life calculation rapidly increases the amount of computational time and for example, prohibits the simplification of the superposition principle.

The influence of load sequence effects on a double K-Joint of a Jacket offshore support structure was shown in an example. The current standard fatigue assessment approach does not exclude load sequence effects but reduces their influence to a minimum by means of conservatism.

Based on the investigations which were carried out, the following steps are desirable to further deepen the insights on load sequence effects.

On part of the numerical calculation, the presented one-dimensional implementation of the UML should be extended to a three dimensional formulation including possibilities to consider mean stress relaxation and mean strain creep. Based on the three-dimensional implementation spatial interference of plastifications should be investigated.

ACKNOWLEDGEMENTS

Parts of the presented investigations were conducted by Mr. Raba during an internship at Vestas Wind Systems A/S in Århus, Denmark. Therefore, the authors kindly acknowledge the support of Marcel van Duijvendijk of Vestas Wind Systems A/S, who facilitated the stay of Mr. Raba in Århus. As well, the authors like to thank Kurt Eigil Juel Pedersen and Jacob Karottki Falk Andersen of Vestas Wind Systems A/S for providing supervision to Mr. Raba during his stay.

REFERENCES

- Bäumel A and Seeger T (1990). "*Materials Data for Cyclic Loading*", Elsevier Science Publishers B.V., Amsterdam.
- Böker, C (2009). "*Load simulation and local dynamics of support structures for offshore wind turbines*", Shaker Verlag, Aachen.
- Clörmann UH and Seeger T (1986). "*HCM – Ein Zählverfahren für Betriebsfestigkeitsnachweise auf werkstoffmechanischer Grundlage*", Stahlbau 55, pp. 65-71, Berlin.
- DNV-OS-J101 (2010). "*Design of offshore wind turbine structures*", Det Norske Veritas, Høvik.
- EN 10225 (2009). "*Weldable structural steels for fixed offshore structures – Technical delivery conditions*", CEN European committee for standardization, Brussels.
- Gudehus H and Zenner H (1999). "*Leitfaden für eine Betriebsfestigkeitsrechnung*", Verlag Stahleisen GmbH, Düsseldorf.
- Haibach E (2006), "*Betriebsfestigkeit – Verfahren und Daten zur Bauteilberechnung*", Springer-Verlag, Berlin.
- Masing G (1926). "*Eigenstressungen und Verfestigung beim Messing*", Proceedings International Congress of Applied Mechanics, pp. 332-335, Zürich.
- Morrow JD (1965). "*Cyclic plastic strain energy and fatigue of metals*", ASTM STP 378, pp. 45-87, Philadelphia Pa.
- Raba A (2011). "*Effects of load sequences in the fatigue performance of welded spatial tubular joints in jackets*", Århus, Denmark.
- Radaj D, Sonsino CM and Fricke W (2006). "*Fatigue assessment of welded joints by local approaches*", Woodhead Publishing Ltd, Cambridge.
- Ramberg W. and Osgood WR (1943). "*Description of stress-strain curves by three parameters - Technical Note No. 902*", National Advisory Committee for Aeronautics, Washington DC.
- Schaumann P, Dubois J, Böker C and Seidel M (2010). "*Integrated simulation of the REpower 5 MW offshore wind turbine with jacket support structure validated by alpha ventus measurement data*", Proceedings of the 10th German Wind Energy Conference DEWEK.
- Smith KN, Watson R and Topper TH (1970). "*A stress-strain function for the fatigue of metals*", J Mater, JMLSA, pp. 767-778.